Nonlinear Dynamics and Neuroscience

Article DOI: 10.18500/0869-6632-003074

Collective dynamics of a neural network of excitable and inhibitory populations: oscillations, tristability, chaos

S. Y. Kirillov[1], *A. A. Zlobin*[1,2], *V. V. Klinshov*[1,2] ✉

[1]Federal Research Center A. V. Gaponov-Grekhov Institute of Applied Physic of the RAS, Nizhny Novgorod, Russia
[2]Lobachevsky State University of Nizhny Novgorod, Russia
E-mail: skirillov@ipfran.ru, sanzlobin@yandex.ru, ✉vladimir.klinshov@ipfran.ru

Received 2.05.2023, accepted 13.07.2023, available online 10.11.2023, published 30.11.2023

The *purpose* of this work is to study the collective dynamics of a neural network consisting of excitatory and inhibitory populations. The *method* of reducing the network dynamics to new generation neural mass models is used, and a bifurcation analysis of the model is carried out. As a *result* the conditions and mechanisms for the emergence of various modes of network collective activity are described, including collective oscillations, multistability of various types, and chaotic collective dynamics. *Conclusion.* The low-dimensional reduced model is an effective tool for studying the essential patterns of collective dynamics in large-scale neural networks. At the same time, the analysis also allows us to elicit more subtle effects, such as the emergence of synchrony clusters in the network and the shifting effect for the boundaries of the existence of dynamical modes.

Keywords: neural networks, collective dynamics, mean-field theory, neural mass models.

Acknowledgements. The work was supported by the Government assignment to the Institute of Applied Physics (Project No. FFUF-2021-0011).

For citation: Kirillov SY, Zlobin AA, Klinshov VV. Collective dynamics of a neural network of excitable and inhibitory populations: oscillations, tristability, chaos. Izvestiya VUZ. Applied Nonlinear Dynamics. 2023;31(6):757–775. DOI: 10.18500/0869-6632-003074

This is an open access article distributed under the terms of Creative Commons Attribution License (CC-BY 4.0).

Introduction

The study of the collective dynamics of large-scale neural networks is one of the important areas necessary for understanding the principles of functioning of the central nervous system and its processing of information. However, the use of realistic detailed network models for these purposes, taking into account the behavior of individual neurons, causes both technical difficulties associated with numerical modeling of large networks, and difficulties with theoretical generalization and interpretation of large volumes of the results obtained. To avoid these difficulties, medium-field models are often used, the so-called neural mass models, which describe the dynamics of a population of neurons in terms of averaged, physically relevant variables, such as the average frequency of generation of action potentials or the average membrane potential. Using such models as "building blocks", it is possible to create meso- and macroscopic models of large-scale neural networks containing many interacting populations from them [1, 2].

© *Kirillov S. Y., Zlobin A. A., Klinshov V. V., 2023*

Recently, the so-called "new generation" of neural mass models [3], which traces its history from the Montbrio-Paso-Roxine model [4], has become increasingly popular in the theoretical modeling of neural systems. The distinctive features of these reduced models are, firstly, the possibility of their strict derivation from equations for microscopic dynamics of neurons, and secondly, their ability not only to describe the average activity of a population, but also to take into account the degree of its synchronization. The latter circumstance is of particular importance for the study of brain rhythms, which are a manifestation of the collective oscillatory activity of neural networks. Thus, new generation neural mass models were used to model gamma rhythms [5], interactions between theta and gamma rhythms [6], the effect of movements on changes in beta rhythms [7]. Models of this type were used to study fluctuations in networks consisting of several populations [8], as well as to model distributed systems—neural fields [9] and the brain as a whole [10, 11].

A neural network consisting of two interacting populations - excitatory and suppressive - is one of the basic fundamental structures (motives) in large-scale brain networks [12–16]. New generation neural mass models have been actively used to study the collective dynamics of such two-population neural networks. Thus, in the work [8], the occurrence of synchronous oscillatory activity in such a network was demonstrated, associated with the transition through the Andronov-Hopf bifurcation in the corresponding reduced model. In the work [17], neural mass models were used to study the occurrence of collective oscillations in balanced neural networks (it should be noted that the medium-field model in this case showed only damped oscillations, whereas self-sustaining oscillations in a microscopic system arose due to finite-size effects). In the work [18], the influence of the populations' own time scales on the fluctuations occurring in the system was investigated. It is shown that, depending on the ratio of the membrane times of the suppressive and excitatory populations, both strongly synchronized (so-called PING) and weakly modulated gamma rhythms can occur. In the work [19] it is shown that the occurrence of collective oscillations in a two-population network can be associated with both the transition through the supercritical and the transition through the subcritical Andronov-Hopf bifurcation in the reduced model. In the work [20], the occurrence of quasi-periodic and chaotic collective oscillations is studied. In [21], cross-frequency synchronization between two populations was investigated. In the work [22], the effect of suppressing vibrations by external influence was studied. In the work [23], the synchronization of periodic collective oscillations by an external periodic signal is studied.

The abundance of work on the dynamics of the neural mass model of a two-population excitatory-suppressive network encourages the systematization and understanding of the results obtained, which served as the initial motivation for this work. However, upon careful study of the system, new, previously undescribed dynamic modes and mechanisms of their occurrence were also discovered in it. Thus, this work represents the first detailed, though not exhaustive, study of the dynamics and bifurcations of the neural mass model of a network consisting of excitatory and suppressive populations.

The work is structured as follows. In the section 1, we formulate a network model and its corresponding neural mass model. In the section 2, the basic case of weak connections is considered, when the dynamics of a two-population model does not qualitatively differ from the dynamics of a single exciting population. In the section 3, the occurrence of collective periodic oscillations is investigated. The section 4 is devoted to the formation of tristability in the system - the coexistence of three stable asynchronous states. The section 5 examines chaotic collective dynamics. In conclusion, the results of the study are summarized briefly.

1. Model

Consider a system consisting of two populations of neurons (populations we will also further call modules when it refers to a reduced system)— excitatory E and suppressive I (hereinafter, the indices e, i determine whether the parameter belongs to the excitatory or suppressive population). Each neuron is described by a quadratic accumulation and reset model

$$V_j = V_j^2 + \eta_j + I_j(t), \tag{1}$$

where V_j is the membrane potential of the jth neuron, η_j is an inhomogeneous bias current, and $I_j(t)$ is the cumulative current received by the jth neuron from other neurons in the network. For each neuron from the population $X = \{e, i\}$, this current is defined as

$$I_X = J_{eX} r_e + J_{iX} r_i, \tag{2}$$

where J_{YX} is the strength of synaptic connections acting on the part of the population Y on the population X, and r_X is the total output signal of the population X, normalized by the number of its elements, and having the meaning of the average frequency of spike generation:

$$r_X(t) = \frac{1}{N_X} \sum_{j \in X} \sum_{k | t_j^k \leqslant t} \delta(t - t_j^k). \tag{3}$$

Here N_X is the number of neurons in the population X. Each jth neuron generates individual spikes at time points t_j^k, which are determined from an additional condition: when the membrane potential of the neuron V_j reaches some predetermined threshold value V_p. After the spike is generated, the potential is reset to the value V_r. Further, we believe that $V_p = -V_r = \infty$.

With a large number of neurons in both populations (in the thermodynamic limit at $N_X \to \infty$), the dynamics of each such population can be approximated using a neural mass model. Let us further assume, for certainty, that the individual displacement currents η_j in each population X are distributed along the Lorentz with the center ζ_X and the half-width Δ_X:

$$g(\eta) = \frac{1}{\pi} \frac{\Delta_X}{\Delta_X^2 + (\eta - \zeta_X)^2}. \tag{4}$$

Then, in the absence of connections between populations, the collective dynamics of each of them can be reduced to the Montbrio-Paso-Roxine system [4]:

$$\begin{aligned} \dot{r}_X &= \frac{\Delta_X}{\pi} + 2 r_X v_X, \\ \dot{v}_X &= v_X^2 + \zeta_X - \pi^2 r_X^2 + J_{XX} r_X, \end{aligned} \tag{5}$$

where the variable r_X models the average frequency of the population X, v_X is its average membrane potential, and J_{XX} is the strength of synaptic connections within the population. When adding connections between populations, the behavior of the complete network will be described by two connected systems of the form (5), that is, the following system of ordinary differential equations:

$$\begin{aligned} \dot{r}_e &= \frac{\Delta}{\pi} + 2 r_e v_e, \\ \dot{v}_e &= v_e^2 + \zeta_e - \pi^2 r_e^2 + J_{ee} r_e + J_{ie} r_i, \\ \dot{r}_i &= \frac{\Delta}{\pi} + 2 r_i v_i, \\ \dot{v}_i &= v_i^2 + \zeta_i - \pi^2 r_i^2 + J_{ii} r_i + J_{ei} r_e. \end{aligned} \tag{6}$$

Further analysis of the collective dynamics of the network is carried out on the basis of a two-module model of neural masses (6).

2. The case of weak intermodule connections

As shown in [4], the intrinsic dynamics of one independent module (5) can be either mono- or bistable. According to the bifurcation diagram shown in Fig. 1, *a*, in this case there may be one or two stable equilibrium states in the system. In a complete (microscopic) system, the bistable mode is characterized by the coexistence of two stable asynchronous modes- with "high" and with "low" the level of average activity. We believe that the connections within the exciting population are positive ($J_{ee} > 0$), and within the overwhelming population are negative ($J_{ii} < 0$). With this choice of parameters, the intrinsic dynamics of the exciting population can be both mono- and bistable, while the overwhelming population always demonstrates a single stable asynchronous state with a low level of activity.

Let's move on to analyzing the dynamics of a two-population network, and for simplicity, let's start with the case of unidirectional communication — only from an exciting population to an overwhelming one ($J_{ei} > 0$, $J_{ie} = 0$). Obviously, in this case, the scenario "master – slave" is implemented, and the dynamics of the system does not differ qualitatively from the case of non-interacting populations. The bifurcation diagram of the corresponding reduced model (6) in this case is identical to the bifurcation diagram for a single exciting module (shown in Fig. 1, *b* with a thin blue line). Let's further assume that the relationship between populations becomes mutual ($J_{ei} > 0$, $J_{ie} < 0$, $|J_{ie}| \ll |J_{ei}|$). Then, at moderate (finite) values of the bond forces J_{ee}, when the "high" state of the exciting population has not too much activity, the result of the interaction of populations is manifested in the bifurcation diagram of the reduced model by only a small shift in the boundaries of the bistability region. For example, let's fix the values of the parameters of the overwhelming population $\zeta_i = -10$, $J_{ii} = -5$ and the values of intermodule connections $J_{ei} = 5$ и $J_{ie} = -1$. The bifurcation diagram on the plane of the parameters ζ_e and J_{ee} for this case is shown in Fig. 1, *b* and shows that even with relatively large values of intermodule bond forces comparable in magnitude to the strength of intramodule bonds, the shape of the bistability region changes slightly compared to the case of unidirectional coupling.

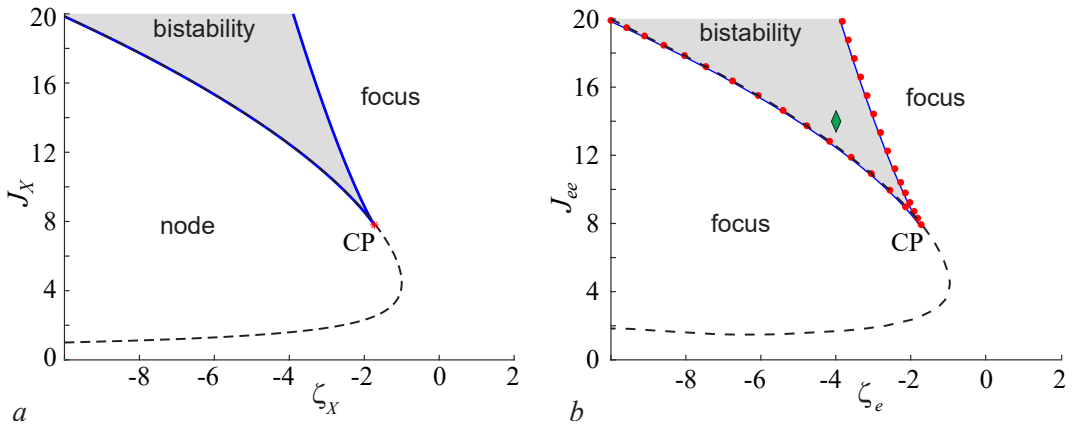

Fig 1. *a* — Two-parameter bifurcation diagram of the Montbrió–Pazó–Roxin system (5) with $\Delta_X = 1$. Bistability region is bounded by two lines of saddle-node bifurcations (blue lines) and has a wedge shape. Dotted line separates the parameter regions for which the stable equilibrium state is either a node or a focus. *b* — Two-parameter bifurcation diagram for the two-module system (6) with unidirectional coupling ($J_{ei} = 5$, $J_{ie} = 0$, $\zeta_i = -10$, $J_{ii} = -5$, thin blue lines) and mutual coupling ($J_{ei} = 5$, $J_{ie} = -1$, $\zeta_i = -10$, $J_{ii} = -5$, red dots). Boundaries of the bistability region are determined by the saddle-node bifurcations. The dotted line separates the parameter regions for which the stable equilibrium state has one or two pairs of complex conjugate characteristic exponents (color online)

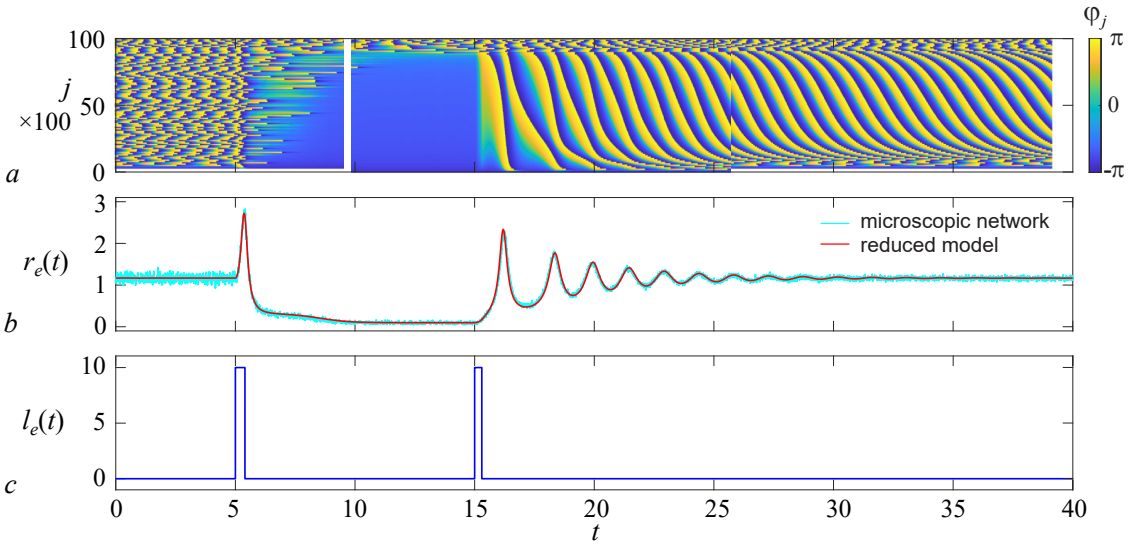

Fig 2. *a* — Spatio-temporal diagram for the excitatory population. The individual phases of each hundredth element are displayed, sorted by the parameter η_j ($\zeta_e = -4$, $J_{ee} = 15$, $J_{ei} = 5$, $J_{ie} = -1$, $\zeta_i = -10$, $J_{ii} = -5$). *b* — Dependence of the average frequency of the excitatory population of the microscopic system (blue line, averaged over a sliding time window $\Delta t = 0.025$) and the macroscopic reduced system (red line). *c* — Sequence of two rectangular current pulses with amplitude $A = 10$, acting on the excitatory population. Duration of the first pulse is $T_1 = 0.4$, and the second one is $T_2 = 0.3$ (color online)

This is due to the fact that at the selected parameter values, the activity of the overwhelming population is very low and it actually plays the role of a passive inertial load. At the same time, despite the fact that the effect of such a load on the asymptotic (stationary) dynamics may not be so noticeable, it can nevertheless significantly affect transient and resonant processes in the system. Indeed, since the only equilibrium state of the free suppressing module is a stable focus, the connection of such a load to the exciting module leads to the appearance of new characteristic frequencies in the system. Thus, damped oscillations in the vicinity of the "low" state of the system are characterized by one frequency, while oscillations in the vicinity of the "high" equilibrium state may contain two incommensurable frequencies.

Let us consider in more detail the behavior of a complete microscopic network, each individual population of which contains $N_{e,i} = 10000$ elements. To do this, we fix the system parameters in the bistability region ($\zeta_e = -4$, $J_{ee} = 15$). The corresponding point on the bifurcation diagram is Fig. 1, *b* is marked with a marker. Then, under the influence of external stimuli, the network can switch between two collective stable states. This process is illustrated in Fig. 2, *a*–*c*.

For the sake of certainty, we assume that at the initial moment of time the system is in a stable "high" asynchronous state. Next, two rectangular current pulses with the same amplitude $A = 10$ and with a duration $T_1 = 0.4$ and $T_2 = 0.3$ (see Fig. 2, *c*). The time interval between pulses is chosen sufficiently large so that macroscopic transients in the system end by the arrival of the second pulse. The collective behavior in this case is well illustrated in Fig. 2, *b*, which shows the dependence of the average frequency of the exciting population on time. As you can see, the action of the first pulse causes the network to switch from a "high" asynchronous state to a "low", while the second pulse restores a high level of network activity. It is interesting to note that a pulse with a duration of T_2 cannot switch the system from a "high" state to a "low", while a pulse with a duration of T_1 does not allow the network to be transferred from a "low" state to "high". Nevertheless, the parameters of the pulse action (amplitude and duration) they can also be selected in such a way that switching between different states will be carried out by the same

pulses. This behavior becomes possible due to the fact that in the case under consideration, the durations of external signals are comparable to the characteristic times of their own macroscopic collective oscillations. All this highlights the importance of a deeper study of transients in a two-population system.

The properties of the natural oscillations of the elements of a microscopic network are illustrated by the space-time diagram shown in Fig. 2, *a*. To build it, it is convenient to go to (1) to new phase variables, using the replacement $V_j = \tan(\varphi_j/2)$, which translates a network of neurons of the accumulation type – reset into an equivalent network of theta neurons. Next, the neurons of the network are ordered in ascending order of the values of their own bias currents η_j, after which every hundredth of them is selected for display on the diagram. As you can see, at the initial stage, most of the elements generate spike vibrations. The analysis shows that the average frequencies of spike generation by individual elements are incommensurable with each other and monotonously increase with an increase in the value of the intrinsic bias current η_j. Accordingly, the phases between any two elements are constantly changing. This leads to mixing of phases throughout the population, which can be observed on the space-time diagram. Next, an external influence switches the system to a new state. The fundamental difference here is that now only a small proportion of the network elements generate spike oscillations, while most of them are in excitable mode. Repeated external influence on the system switches it back to a state with high spike activity. In this case, some of the elements are excited with close phases, which leads to pronounced attenuating macroscopic oscillations reflecting a decrease in the proportion of network elements generating spikes at the same time. Note that according to Fig. 2, *b* macroscopic activity reaches a stationary level relatively quickly, while in the space-time diagram Fig. 2, *a* traveling wave fronts continue to be observed within the population. This is due to the fact that elements with values of η_j in the vicinity of the average value of ζ_e have, although different, but still very close frequencies. As a result, it takes much longer to mix the phases of individual elements (as can be observed at the initial stage).

3. The emergence of self-sustaining collective fluctuations

Let's now consider how the dynamics of the reduced system (6) will change with an increase in the strength of the intermodule coupling J_{ei}. At moderate values, for example $J_{ei} = 12$, the shape of the bistability wedge still does not change significantly. However, additional qualitatively new modes arise in the system, namely periodic fluctuations. The mechanism of occurrence of these oscillations is associated with an amplification of the feedback loop arising from the exciting module through the suppressor, as a result of which the "high" equilibrium state is destabilized. As shown in the two-parameter diagram (Fig. 3), the limit cycle corresponding to fluctuations can occur through the Andronov-Hopf bifurcation (AH), and then undergo other bifurcations, including disappearing through the bifurcation of the saddle separatrix loop (H) or the bifurcation of the double limit cycle (LPC).

Let's consider several scenarios for the occurrence of fluctuations, and to do this, we will build a series of one-parameter diagrams for various fixed values of the binding force J_{ee}. With a sufficiently strong coupling, for example $J_{ee} = 16.4$, oscillations are generated through the supercritical Andronov-Hopf bifurcation, which undergoes a high equilibrium state when the average current increases to the value $\zeta_e = -6.578 \pm 10^{-3}$. The resulting stable limit cycle undergoes a bifurcation of the saddle separatrix loop at $\zeta_e = -6.258 \pm 10^{-3}$ with a further increase in the average current. A further increase in the average current leads to a repeated bifurcation of the separatrix loop at $\zeta_e = -5.891 \pm 10^{-3}$, in which a stable limit cycle is born

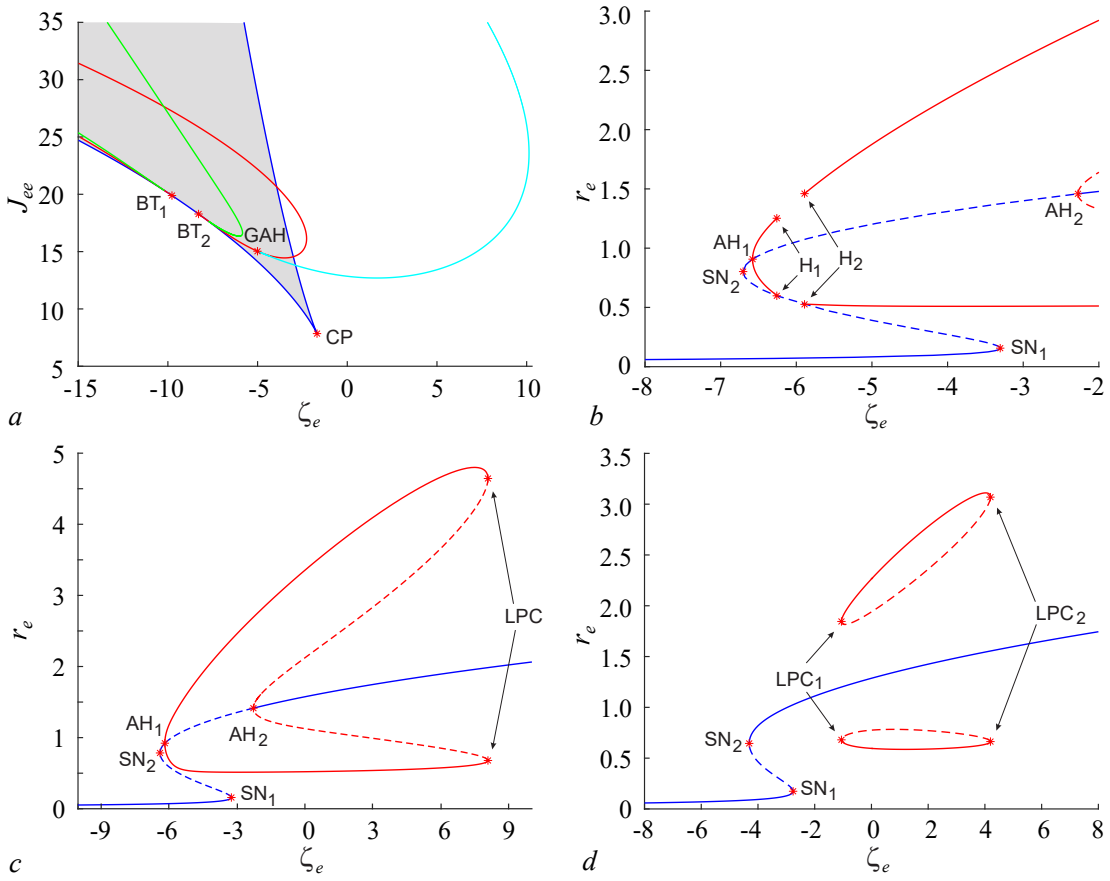

Fig 3. *a* — Two-parameter bifurcation diagram of the two-module system (6) with $J_{ei} = 12$, $\zeta_i = -10, J_{ii} = -5$, $J_{ie} = -1$. Gray color indicates the area in which system (6) contains three equilibrium states. The curves corresponding to Andronov–Hopf bifurcations are marked in red. The bifurcation lines of the separatrix loop of the saddle are marked in green. The cyan line corresponding to the double limit cycle. The asterisks mark bifurcations of codimension 2: two Bogdanov–Takens bifurcations and the Bautin (generalized Andronov–Hopf, GAH) bifurcation. *b–d* — One-parameter bifurcation diagrams of the two-population network (6) with $J_{ee} = 16.4$ (*b*), 16.0 (*c*), 13.1 (*d*). Asterisks mark the points of saddle-node bifurcations of equilibrium states (SN), Andronov–Hopf bifurcations (AH), bifurcations of the saddle separatrix loop (H) and double limit cycle (LPC). Blue lines correspond to equilibrium states, while red lines correspond to limit cycles (color online)

again. Thus, in the range of bias currents $-6.258 < \zeta_e < -5.891$, the disappearance of oscillations is observed, and there are no stable high states in the system - both stationary and oscillatory.

With a lower coupling strength, for example $J_{ee} = 16.0$, fluctuations also occur through the supercritical Andronov-Hopf bifurcation at $\zeta_e = -6.173 \pm 10^{-3}$, however, the disappearance of the limit cycle through the saddle separatrix loop does not occur. And further, when the current increases to $\zeta_e = -2.270 \pm 10^{-3}$, a subcritical Andronov-Hopf bifurcation occurs, as a result of which the high equilibrium state is stabilized, and an unstable limit cycle is separated from it. With a further increase in current to $\zeta_e = 8.065 \pm 10^{-3}$, the unstable limit cycle merges with the stable one as a result of bifurcation of the two-fold limit cycle. Thus, in the range of currents $-2.270 < \zeta_e < 8.065$, two high states coexist in the system - stationary and oscillatory.

With an even lower bond strength, for example $J_{ee} = 13.1$, the Andronov-Hopf bifurcation is not observed, and a high equilibrium state is always stable. In this case, the birth of oscillatory states occurs through the bifurcation of a two-fold limit cycle at $\zeta_e = -1.058 \pm 10^{-3}$, and when the current increases to $\zeta_e = 4.195 \pm 10^{-3}$, the oscillatory states disappear through the same

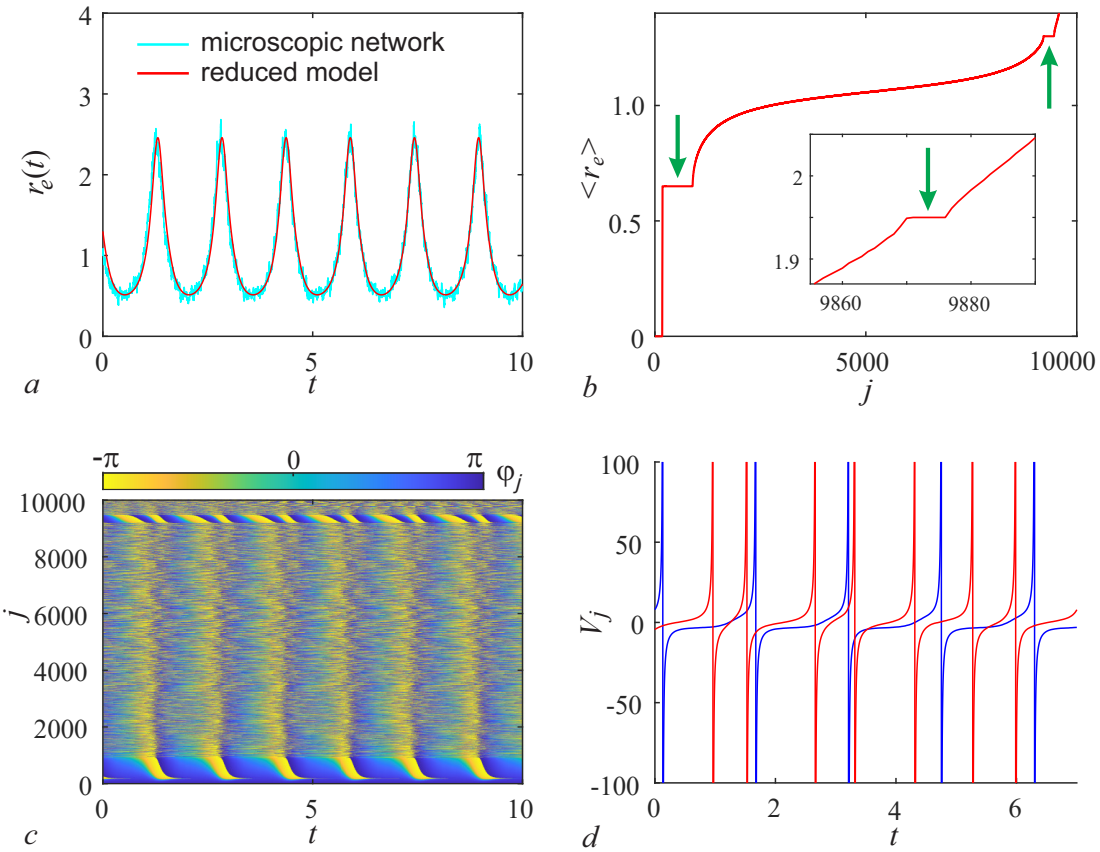

Fig 4. *a* — Collective oscillations of the microscopic system (1) (light blue line) and the macroscopic reduced system (6) (red line). *b* — The average frequency of the elements of the excitatory population, sorted by increasing η_j. *c* — Spatio-temporal diagram of the excitatory population in the regime of collective oscillations. *d* — Voltage time traces of two elements of the excitatory population: periodic oscillations of an element from the first synchronous cluster (blue line, $j = 200$) and non-periodic oscillations of an element not included in synchronous clusters (red line, $j = 8000$). Parameters: $\zeta_e = -3$, $J_{ee} = 16.0$, $J_{ei} = 12$, $\zeta_i = -10$, $J_{ii} = -5$, $J_{ie} = -1$ (color online)

bifurcation.

Let's move on to the analysis of collective oscillations occurring in a microscopic network. For certainty, we choose the values of the parameters $\zeta_e = -3$, $J_{ee} = 16.0$, $J_{ei} = 12$, $\zeta_i = -10, J_{ii} = -5$, $J_{ie} = -1$ (Fig. 3, *c*). In this case, the complete system implements a mode of generating stable periodic collective oscillations. This process is illustrated in Fig. 4, *a*. As can be seen from the figure, the results of modeling micro- and macroscopic systems demonstrate good qualitative and quantitative correspondence.

Let us consider in more detail the properties of vibrations of individual elements of the exciting population of a microscopic network. The average frequencies of these oscillations are $\langle r_e(j) \rangle$ are shown in Fig. 4, *b*. In this case, all elements of the population are ordered in ascending order of the magnitude of the individual displacement currents η_j. It can be seen that almost all elements of the network, with the exception of only a small number of them, generate spikes with some non-zero natural frequencies. Note that there is a cluster of elements in the system that oscillate at a single frequency $\omega_j = \omega_m = 0.67 \pm 0.01$, which coincides with the frequency of macroscopic oscillations of the mean field. In addition, it is also possible to detect two more synchronous clusters, the elements of which oscillate at a doubled $\omega_j = 2\omega_m$ and a tripled $\omega_j = 3\omega_m$ frequency of collective oscillations.

Let us now proceed to the analysis of the space-time diagram shown in Fig. 4, *c*. It shows

the first synchronous cluster in the low frequency region, as well as the second synchronous cluster in the high frequency region. The third synchronous cluster is not visible on the scale shown in the figure due to the small number of elements included in it (7 elements). As shown in Fig. 4, *c*, despite the fact that the elements inside synchronous clusters oscillate with the same average frequency, the properties of such oscillations are different. These differences are manifested both in the moments of occurrence of their own spikes (which can be in different phase ratios with fluctuations in the mean field), and in the times that individual elements spend in one or another phase of oscillations.

Note that according to Fig. 4, *b* the average frequencies of elements outside synchronous clusters vary from element to element and are incommensurable. At the same time, in Fig. 4, *c* it can be seen that there is an obviously visible regular component in these fluctuations. This behavior is made possible by the fact that fluctuations outside synchronous clusters can be non-periodic. This is illustrated in Fig. 4, *d*, which shows spike vibrations of two elements: vibrations of an element from the first synchronous cluster ($n_j = 200$) and an element outside synchronous clusters ($n_j = 8000$).

4. Tristability of collective asynchronous states

So far, we have considered situations where the action of intermodule connections does not change the number of equilibrium states in a reduced system (6) and has little effect on the shape of the regions of their existence in the parameter space. However, other situations are possible. To study them, we select new fixed values of the parameters of the suppressive module $\zeta_i = -2.5247$, $J_{ii} = -0.2313$, $J_{ie} = -5.0777$ and investigate how the two-parameter bifurcation diagram changes on the plane $O(\zeta_e, J_{ee})$ depending on the strength connections J_{ei}.

With a relatively small bond strength, $J_{ei} = 1$ the system (6) can only undergo saddle-node bifurcations leading to bistability, as described in section 2. In this case, the two-parameter bifurcation diagram qualitatively corresponds to Fig. 1, *b*. With an increase in the bond strength to $J_{ei} = 7$, stable fluctuations may occur in the system, described in the section 3. The two-parameter bifurcation diagram looks similar to Fig. 3, *a*. With a further increase in the binding force to $J_{ei} = 10$, the two Bogdanov-Takens points merge and disappear, after which the bifurcation curves of limit cycles do not contain more common points with the bifurcation curves of equilibrium states (Fig. 5, *a*).

With a subsequent increase in J_{ei}, one can observe how a fracture and self-intersection occur on the left line of the saddle-node bifurcation (Fig. 5, *b*). At the same time, a triangular tristability region arises inside the wedge-shaped bistability region with three stable equilibrium states of the focus type (with one or two pairs of complex conjugate Lyapunov characteristic indicators) and two equilibrium states of the saddle focus type (with one pair of real Lyapunov characteristic indicators of different signs and one pair of complex conjugate indicators with a negative real part). A further increase in J_{ei} causes the triangular region of tristability to shift to the top of the wedge, where its shape transforms into a quadrangular one (Fig. 5, *c*). With a subsequent increase in J_{ei}, the tristability region rises up along the right edge of the wedge and then disappears.

In the field of tristability, there are three stable equilibrium states in the system — in addition to the "low" and "high" states, a third, "medium" state is formed. Stable equilibrium states are separated by saddle-focus equilibrium states and merge with them in saddle-node bifurcations at the boundaries of the tristability region. A typical scenario of the occurrence of tristability is illustrated on a one-parameter bifurcation diagram (Fig. 6, *a*). When the

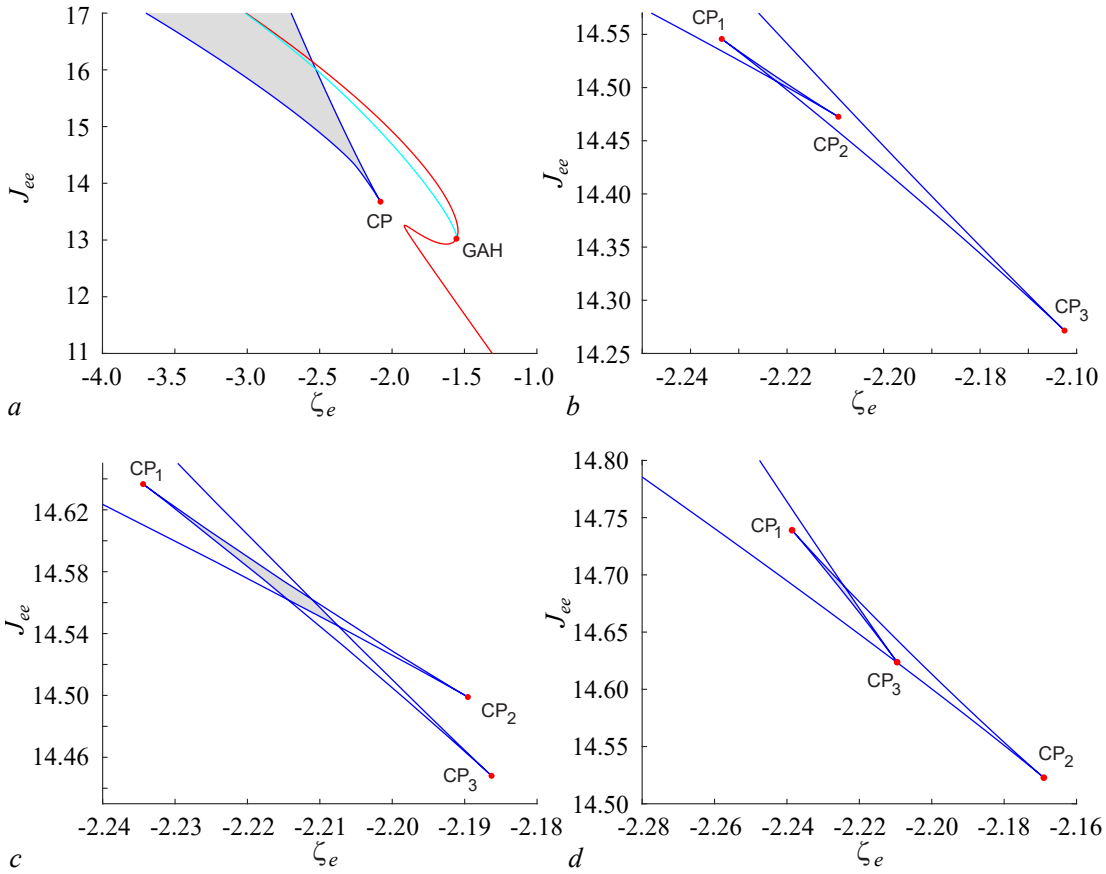

Fig 5. *a* — Two-parameter bifurcation diagram of the two-module system (6). The saddle-node bifurcation of equilibrium states is marked in dark blue, Andronov–Hopf bifurcation is marked in red, and the double limit cycle bifurcation is marked in light blue. The dots denote bifurcations of codimension two: the cusp point and the Bautin (generalized Andronov–Hopf) point. Parameter: $\zeta_i = -2.5247$, $J_{ii} = -0.2313$, $J_{ie} = -5.0777$; $J_{ei} = 10.2$ (*a*), 10.67 (*b*), 10.8089 (*c*), 10.9478 (*d*) (color online)

displacement current increases to the value $\zeta_e = -2.22061 \pm 10^{-5}$, an average stable equilibrium state occurs through the saddle-node (SN) bifurcation, and the system becomes bistable. At $\zeta_e = -2.21986 \pm 10^{-5}$, a second saddle-node bifurcation occurs, a high state is born, and the system becomes tristable. Next, the average state disappears at $\zeta_e = -2.21886 \pm 10^{-5}$, and the system is bistable again. At $\zeta_e = -2.21146 \pm 10^{-5}$, the low state disappears and the system becomes monostable.

In the above case, the tristability region turned out to be quite narrow (on the order of $3 \cdot 10^{-3}$ according to the parameter ζ_e), while all the modes predicted by the reduced model are observed in a microscopic system. However, it should be noted that there are differences between the bifurcation boundaries of the dynamic regimes of the reduced system (fair in the thermodynamic limit $N \to \infty$) and the regions of existence of the corresponding dynamic regimes of the complete network. These differences are less noticeable the larger the network size, but they remain noticeable even for fairly large networks, as shown in Fig. 6, *a* for $N_X = 200,000$. A similar effect of shifting the boundaries of the existence of dynamic modes in finite-size networks was observed earlier in a network consisting of a single population of neurons [24].

By changing the parameters of the suppressive module, the width of the tristability region can be significantly increased. At the same time, the presence of additional bifurcations associated with the emergence of periodic solutions is characteristic for cases of a wider tristability domain.

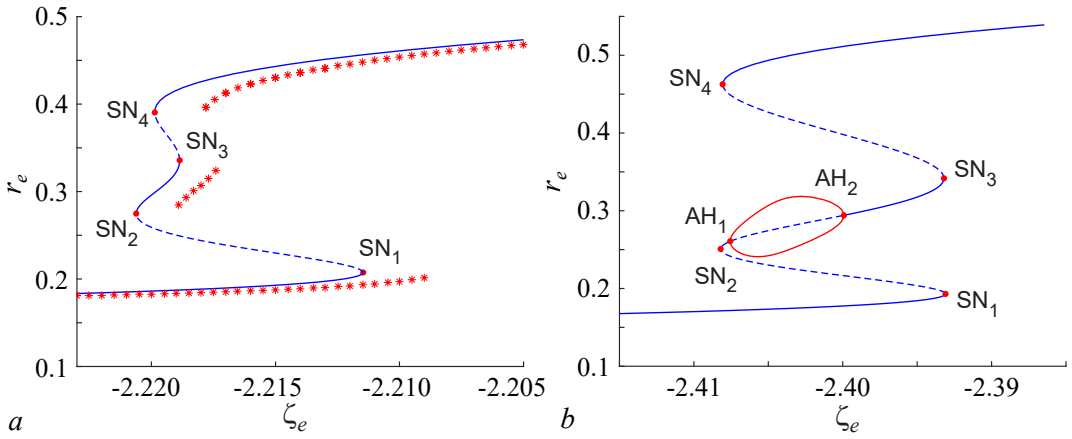

Fig 6. A one-parameter bifurcation diagram of the two-module system (6) in the region of tristability of equilibrium states (blue line). Red asterisks indicate dynamic modes found in the microscopic network (1). Parameters: $N_e = N_i = 200000$, $\zeta_i = -2.5247$, $J_{ii} = -0.2313$, $J_{ie} = -5.0777$, $J_{ee} = 14.50$, $J_{ei} = 10.67$. *b* — A one-parameter bifurcation diagram of the two-module (6) system in the tristability region with a partially synchronous medium activity state. Parameters: $\zeta_i = -2.8265$, $J_{ii} = -0.2313$, $J_{ie} = -5.4552$, $J_{ee} = 15.6404$, $J_{ei} = 11.9226$ (color online)

For example, in Fig. 6, *b* shows a one-parameter bifurcation diagram in which the tristability region has a width of about 0.02 according to the parameter ζ_e, but at the same time, within the interval of existence of the average equilibrium state, it destabilizes and generates a stable oscillatory state. To build two-parameter diagrams in Fig. 5 deliberately selected parameters for which the tristability region is narrow, because in this way it is possible to avoid imposing bifurcations of limit cycles on this region. Otherwise, bifurcation diagrams become extremely difficult to perceive, since many bifurcation curves can be localized in narrow parameter regions.

An analysis of the collective dynamics of the complete system in the field of tristability has shown that a microscopic system can be in one of three stable asynchronous modes. In this case, in addition to the collective macroscopic states, when most of the network elements are in excitable mode or in spike generation mode, a state is added when the number of active and inactive elements is comparable in magnitude. Qualitatively, the behavior of individual elements in this case does not differ from what was discussed earlier, so here we do not dwell on this issue in more detail.

5. The emergence of collective chaotic fluctuations

In addition to stationary and periodic modes, more complex dynamic modes, including chaotic oscillations, can occur in a two-module network. To study them, we fix the values of the parameters of the suppressive module $\zeta_i = 3.4$, $J_{ii} = -5.9$, $J_{ie} = -13.9$. With a sufficiently weak effect of the exciting population on the suppressive one ($J_{ei} \ll 1$), only saddle-node bifurcations are possible in the system and the two-parameter bifurcation diagram has a form that qualitatively coincides with Fig. 1, *b*. With an increase in the strength of the intermodule communication in the system, it becomes possible to create stable periodic solutions, similar to how it is described in the section 3. For sufficiently large values, for example $J_{ei} = 1.0$, these periodic solutions can exhibit period doubling bifurcations, as shown in Fig. 7, *a*. Note that this figure shows only the line of the first doubling, whereas inside the area bounded by it there is a whole family of nested bifurcation curves of doubling the period. The presence of such a family suggests the possibility of the birth of a strange chaotic attractor according to the Feigenbaum

scenario [25].

This scenario is indeed observed in the system, as illustrated in Fig. 7, *b*, where a one-parameter diagram is shown for a fixed $J_{ee} = 16.8$. In this case, the high equilibrium state is destabilized through the Andronov-Hopf bifurcation at $\zeta_e = -0.94 \pm 10^{-2}$. The resulting stable limit cycle undergoes the first period doubling bifurcation (PD) at $\zeta_e = -0.3 \pm 10^{-2}$, the second at $\zeta_e = 0.12 \pm 10^{-2}$. Subsequent bifurcations accumulate at $\zeta_e = 0.63 \pm 10^{-2}$, and a chaotic attractor appears in the system. It continues to exist up to $\zeta_e = 1.06 \pm 10^{-2}$ (except for narrow windows of periodicity), after which it disappears through a reverse cascade of doubling.

To confirm the chaotic nature of the attractor, two senior Lyapunov exponents were calculated, shown in Fig. 7, *c*. It can be seen that in the chaotic region of $0.63 < \zeta_e < 1.06$, the senior indicator is really positive. A characteristic phase portrait of the chaotic attractor is shown in Fig. 7, *d*.

Note that with higher values of J_{ee}, additional bifurcations are possible in the system, not shown in Fig. 7, *a* to facilitate its perception. At the same time, more complex scenarios of the emergence and disappearance of chaos are realized, including those associated with touching invariant manifolds of saddle limit cycles, as well as multistable chaos. A full understanding of such scenarios requires additional research.

Next, we will show how the chaotic oscillations of the reduced system (6) we have considered manifest themselves in a complete microscopic system (1). As shown in Fig. 8, in this case, collective chaotic fluctuations occur in the system (1). In Fig. 8, *a* these oscillations are represented on the plane of the average frequencies of the exciting and suppressing populations (r_e, r_i). It can be seen that, on average, a macroscopic reduced system reproduces the collective oscillations of a microscopic network quite well. At the same time, the trajectory corresponding to collective microscopic fluctuations contains clearly visible fluctuations. The existence of such fluctuations is associated with finite-size effects. With an increase in the number of elements, the intensity of fluctuations decreases inversely proportional to the size of the network and the trajectories of the reduced and microscopic systems asymptotically converge.

An analysis of the behavior of individual network elements shows that despite the fact that their collective dynamics is irregular, they can nevertheless form clusters with the same average spike generation frequencies. This is illustrated in Fig. 8, *b*, which shows the distribution of the average frequencies of spike oscillation generation across the elements of the exciting population, ordered in ascending order of individual bias currents η_j. As you can see, only a small number of network elements are in excitable mode, while most of them perform spike oscillations at various frequencies. Note that two large clusters arise in the system, the elements of which have the same average frequencies. Fluctuations in them occur at a frequency of $\omega_1 = 0.459 \pm 0.001$ and at a doubled frequency of $\omega_2 = 2\omega_1$. In addition, numerical modeling also shows a small cluster of elements at some intermediate frequency $\omega_3 \approx 1.5\omega_1$, in the vicinity of which elements with relatively close but different frequencies from ω_3 are also grouped.

The properties of oscillations of a microscopic system depending on time are illustrated by the space-time diagram shown in Fig. 8, *c*. The area corresponding to the first cluster at the frequency ω_1 is clearly visible. In this case, spikes occur in pairs: a shorter spike interval is followed by a longer one and vice versa. Next, you can highlight the area in which spikes occur in threes. It corresponds to fluctuations of elements near the cluster with a frequency of ω_3. Activity in a cluster with a frequency of ω_2 is characterized by two pairs of spikes following each other, after which the pattern repeats. The vibrations of the elements outside the clusters have incommensurable frequencies, which is reflected in the blurriness of the corresponding regions on the space-time diagram.

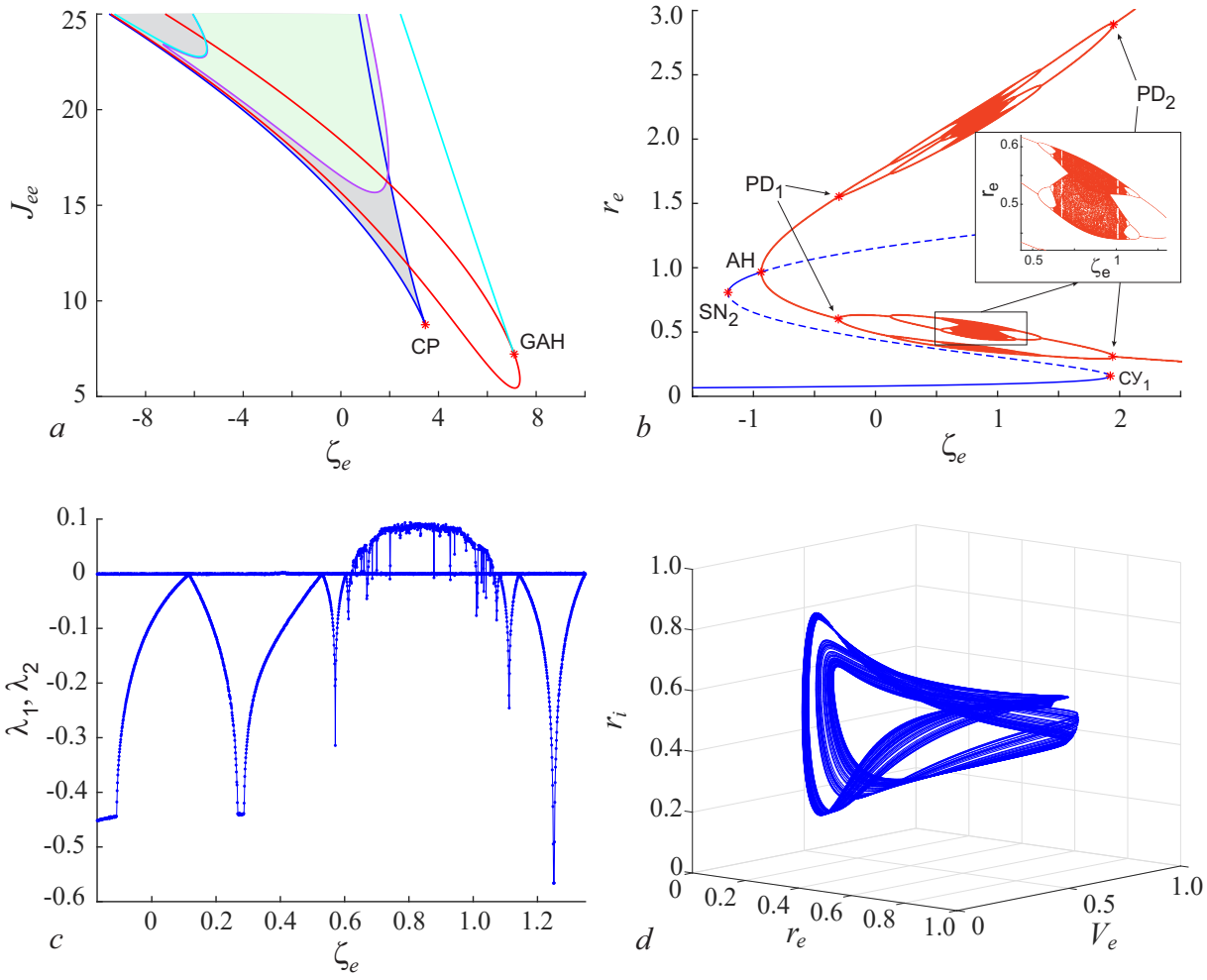

Fig 7. *a* — Two-parameter bifurcation diagram of the two-module system (6). The curves corresponding to saddle-node bifurcations of equilibrium states are marked in blue. The curves corresponding to Andronov–Hopf bifurcations are marked in red. The curves corresponding to the bifurcations of the double limit cycle are marked in light blue. The lilac color indicates the curve corresponding to the period doubling (PD) bifurcation. The area covered by this curve is highlighted in green. The asterisks mark the bifurcations of codimension 2: the cusp point (CP) and the Bautin (generalized Andronov–Hopf, GAH) bifurcations. Parameters: $J_{ei} = 1.0$, $\zeta_i = 3.4$, $J_{ii} = -5.9$, $J_{ie} = -13.9$. *b* — One-parameter bifurcation diagram of the two-module system (6) with $J_{ee} = 16.8$. Blue lines indicate equilibrium states, red lines indicate periodic and chaotic oscillations. *c* — Dependence of the first two Lyapunov exponents on the bias current ζ_e. *d* — A chaotic attractor of the system with $\zeta_e = 0.8$ (color online)

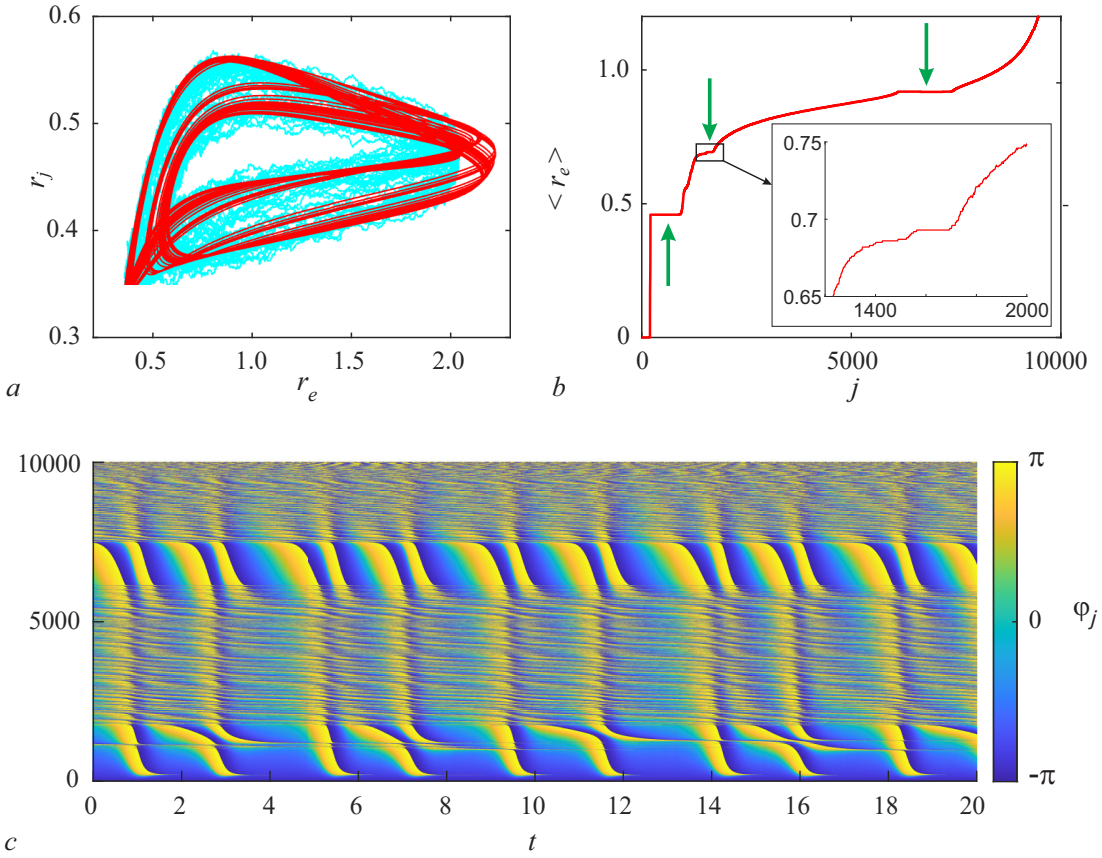

Fig 8. *a* — Projection of the collective chaotic oscillations of the system (1) onto the plane (r_e, r_i) (cyan line, averaged over a sliding time window $\Delta t = 0.025$) and the corresponding projection of the chaotic oscillations of the reduced system (6) (red line). *b* — The average frequency of the elements of the excitatory population, sorted in ascending order η_j. *c* — Spatiotemporal diagram of the excitatory population in the regime of chaotic collective oscillations. Parameters: $N_e = 10000$, $N_i = 10000$, $\zeta_e = 0.8$, $J_{ee} = 16.8$, $J_{ei} = 1.0$, $\zeta_i = 3.4$, $J_{ii} = -5.9$, $J_{ie} = -13.9$ (color online)

Conclusion

In this article, the collective dynamics of a two-population neural network consisting of excitatory and suppressive populations of quadratic neurons of the accumulation–reset type is investigated. Assuming Lorentzian heterogeneity of the parameters of both populations, their dynamics can be reduced to a system of two related models of neural masses. The resulting dynamic system has a relatively low dimension (equal to four), which made it possible to apply bifurcation analysis methods to it.

It is shown that, depending on the parameters, the system can exhibit various collective modes, namely: bistability with the coexistence of high and low equilibrium states; periodic oscillations that can coexist with one or two equilibrium states; tristability of three equilibrium states; chaotic oscillations. The dynamic mechanisms of the emergence of the described collective regimes are studied in detail. To describe these mechanisms, the method of bifurcation diagrams was used, while the parameters of the overwhelming population ζ_i, J_{ii}, J_{ie} were fixed and two-parameter bifurcation diagrams were constructed on the plane of the parameters of the exciting population ζ_e, J_{ee} with a sequential increase in the intermodule coupling J_{ei}. Thus, with zero intermodule coupling, the bifurcation diagram has a simple shape and contains only a wedge of

bistability bounded by two saddle-node bifurcations. A consistent increase in the intermodule connection made it possible to trace the occurrence of additional bifurcation curves and describe their patterns.

The dynamics of the reduced model and the collective dynamics of the complete system were also compared. It is shown that the reduced model approximates the dynamics of large networks well, in which each population includes $N = 10,000$ neurons. Collective fluctuations, both regular and chaotic, lead to the emergence of clusters of synchronous activity of neurons in the network. The effect of shifting the boundaries of the existence of regimes in reduced and complete systems is also found, especially clearly noticeable in the case of tristability for the "average" equilibrium state existing in a rather narrow range of parameters.

Note that in the study of various effects (fluctuations, tristability, chaos), the fixed values of the parameters of the overwhelming population $(\zeta_i, J_{ii}, J_{ie})$ were chosen differently. This inconvenience is due to the desire to separate these effects, since the possibility of observing all three effects at the same parameter values of the overwhelming population exists, but they will all be observed simultaneously, which makes it extremely difficult to perceive the corresponding bifurcation diagrams.

References

1. Deco G, Jirsa VK, Robinson PA, Breakspear M, Friston K. The dynamic brain: From spiking neurons to neural masses and cortical fields. PLoS Comput. Biol. 2008;4(8):e1000092. DOI: 10.1371/journal.pcbi.1000092.
2. Schwalger T, Deger M, Gerstner W. Towards a theory of cortical columns: From spiking neurons to interacting neural populations of finite size. PLoS Comput. Biol. 2017;13(4): e1005507. DOI: 10.1371/journal.pcbi.1005507.
3. Coombes S, Byrne Á. Next generation neural mass models. In: Corinto F, Torcini A, editors. Nonlinear Dynamics in Computational Neuroscience. PoliTO Springer Series. Cham: Springer; 2019. P. 1–16. DOI: 10.1007/978-3-319-71048-8_1.
4. Montbrió E, Pazó D, Roxin A. Macroscopic description for networks of spiking neurons. Phys. Rev. X. 2015;5(2):021028. DOI: 10.1103/PhysRevX.5.021028.
5. Devalle F, Roxin A, Montbrió E. Firing rate equations require a spike synchrony mechanism to correctly describe fast oscillations in inhibitory networks. PLoS Comput. Biol. 2017; 13(12):e1005881. DOI: 10.1371/journal.pcbi.1005881.
6. Bi H, Segneri M, di Volo M, Torcini A. Coexistence of fast and slow gamma oscillations in one population of inhibitory spiking neurons. Phys. Rev. Research. 2020;2(1):013042. DOI: 10.1103/PhysRevResearch.2.013042.
7. Byrne Á, Brookes MJ, Coombes S. A mean field model for movement induced changes in the beta rhythm. Journal of Computational Neuroscience. 2017;43(2):143–158. DOI: 10.1007/10827-017-0655-7.
8. Schmidt H, Avitabile D, Montbrió E, Roxin A. Network mechanisms underlying the role of oscillations in cognitive tasks. PLoS Comput. Biol. 2018;14(9):e1006430. DOI: 10.1371/journal.pcbi.1006430.
9. Byrne Á, Ross J, Nicks R, Coombes S. Mean-field models for EEG/MEG: From oscillations to waves. Brain Topography. 2022;35(1):36–53. DOI: 10.1007/s10548-021-00842-4.
10. Gerster M, Taher H, Škoch A, Hlinka J, Guye M, Bartolomei F, Jirsa V, Zakharova A, Olmi S. Patient-specific network connectivity combined with a next generation neural mass model to test clinical hypothesis of seizure propagation. Frontiers in Systems Neuroscience. 2021;15:675272. DOI: 10.3389/fnsys.2021.675272.

11. Lavanga M, Stumme J, Yalcinkaya BH, Fousek J, Jockwitz C, Sheheitli H, Bittner B, Hashemi M, Petkoski S, Caspers S, Jirsa V. The virtual aging brain: a model-driven explanation for cognitive decline in older subjects. bioRxiv 2022.02.17.480902. DOI: 10.1101/2022.02.17.480902.
12. Wilson HR, Cowan JD. Excitatory and inhibitory interactions in localized populations of model neurons. Biophysical Journal. 1972;12(1):1–24. DOI: 10.1016/S0006-3495(72)86068-5.
13. van Vreeswijk C, Sompolinsky H. Chaos in neuronal networks with balanced excitatory and inhibitory activity. Science. 1996;274(5293):1724–1726. DOI: 10.1126/science.274.5293.1724.
14. Brunel N. Dynamics of sparsely connected networks of excitatory and inhibitory spiking neurons. Journal of Computational Neuroscience. 2000;8(3):183–208. DOI: 10.1023/A:1008925309027.
15. Maslennikov OV, Kasatkin DV, Rulkov NF, Nekorkin VI. Emergence of antiphase bursting in two populations of randomly spiking elements. Phys. Rev. E. 2013;88(4):042907. DOI: 10.1103/PhysRevE.88.042907.
16. Maslennikov OV, Nekorkin VI. Modular networks with delayed coupling: Synchronization and frequency control. Phys. Rev. E. 2014;90(1):012901. DOI: 10.1103/PhysRevE.90.012901.
17. di Volo M, Torcini A. Transition from asynchronous to oscillatory dynamics in balanced spiking networks with instantaneous synapses. Phys. Rev. Lett. 2018;121(12):128301. DOI: 10.1103/PhysRevLett.121.128301.
18. Keeley S, Byrne Á, Fenton A, Rinzel J. Firing rate models for gamma oscillations. Journal of Neurophysiology. 2019;121(6):2181–2190. DOI: 10.1152/jn.00741.2018.
19. Segneri M, Bi H, Olmi S, Torcini A. Theta-nested gamma oscillations in next generation neural mass models. Frontiers in Computational Neuroscience. 2020;14:47. DOI: 10.3389/fncom.2020.00047.
20. Bi H, di Volo M, Torcini A. Asynchronous and coherent dynamics in balanced excitatory-inhibitory spiking networks. Frontiers in Systems Neuroscience. 2021;15:752261. DOI: 10.3389/fnsys.2021.752261.
21. Ceni A, Olmi S, Torcini A, Angulo-Garcia D. Cross frequency coupling in next generation inhibitory neural mass models. Chaos: An Interdisciplinary Journal of Nonlinear Science. 2020;30(5):053121. DOI: 10.1063/1.5125216.
22. Pyragas K, Fedaravičius AP, Pyragienė T. Suppression of synchronous spiking in two interacting populations of excitatory and inhibitory quadratic integrate-and-fire neurons. Phys. Rev. E. 2021;104(1):014203. DOI: 10.1103/PhysRevE.104.014203.
23. Reyner-Parra D, Huguet G. Phase-locking patterns underlying effective communication in exact firing rate models of neural networks. PLoS Comput. Biol. 2022;18(5):e1009342. DOI: 10.1371/journal.pcbi.1009342.
24. Klinshov VV, Smelov PS, Kirillov SY. Constructive role of shot noise in the collective dynamics of neural networks. Chaos: An Interdisciplinary Journal of Nonlinear Science. 2023;33(6):061101. DOI: 10.1063/5.0147409.
25. Feigenbaum MJ. Quantitative universality for a class of nonlinear transformations. Journal of Statistical Physics. 1978;19(1):25–52. DOI: 10.1007/BF01020332.